

Traversable wormhole sourced by a generalized string fluid in the 4D Einstein-Gauss-Bonnet gravity

C. R. Muniz,^{1,*} Milko Estrada,^{2,†} M. S. Cunha,^{3,‡} and L. C. N. Santos^{4,§}

¹*Universidade Estadual do Ceará, Faculdade de Educação, Ciências e Letras de Iguatu, 63500-000, Iguatu, CE, Brazil.*

²*Facultad de Ingeniería y Empresa, Universidad Católica Silva Henríquez, Chile*

³*Universidade Estadual do Ceará (UECE),*

Centro de Ciências e Tecnologia (CCT), 60714-903, Fortaleza-CE, Brazil

⁴*Departamento de Física, CFM - Universidade Federal de Santa Catarina; C.P. 476, CEP 88.040-900, Florianópolis, SC, Brasil*

Abstract

We investigate traversable wormhole solutions in four-dimensional Einstein-Gauss-Bonnet (EGB) gravity coupled with a generalized string fluid background. Our analysis reveals that zero-tidal solutions meet all geometric criteria for traversability while avoiding singularities, with the Gauss-Bonnet coupling α modulating the throat geometry and asymptotic behavior. Varying the parameters α and ε significantly affects curvature both near the throat and at large distances, maintaining finite values throughout spacetime. We demonstrate that the null energy condition (NEQ) can be satisfied for high values of α ($\gtrsim 1$) and low string fluid density ε ($\lesssim 0.1$), greatly reducing the exotic matter requirement compared to general relativistic wormholes. The string fluid's behavior approaches that of a cloud of strings for large α or ε . Additionally, the volume integral quantifier and complexity factor analyses show that increasing α reduces gravitational complexity and exotic matter content near the throat, aligning with NEQ preservation. Our results establish that the combined influence of Gauss-Bonnet gravity and string-like matter can support traversable wormholes while minimizing unphysical energy conditions, offering new insights for constructing viable wormhole geometries in modified gravity.

PACS numbers: 72.80.Le, 72.15.Nj, 11.30.Rd

* celio.muniz@uece.br

† milko.estrada@gmail.com

‡ marcony.cunha@uece.br

§ luis.santos@ufsc.br

I. INTRODUCTION

To explain the phenomenon of cosmic acceleration, a dominant contribution from a homogeneously distributed fluid with negative pressure has usually been invoked, commonly known as dark energy. In this context, a common explanation for this phenomenon has been the presence of the cosmological constant. However, the latter has posed several challenges, such as the cosmological constant problem and the coincidence problem. Along these lines, an alternative explanation for the phenomenon of cosmic acceleration has been to replace the cosmological constant with a scalar field known as quintessence, which evolves within a suitably chosen self-interaction potential. This approach has provided theoretical insights into the cosmological constant problem [1]. However, there do not appear to be successful attempts to address the coincidence problem, as it requires overly stringent constraints on the potential, leading to a fine-tuning problem [2].

In connection with the previous paragraphs, an alternative possibility is presented in Reference [3], where the energy-momentum tensor takes the form of a generalized string fluid. The energy-momentum tensor of a generalized string fluid in a given spacetime can be effectively interpreted as an anisotropic fluid, meaning that the pressure within the fluid varies depending on the spatial direction. In particular, in Reference [4], within the context of regular black holes, a generalized string fluid is defined as one in which the tangential pressure follows the equation of state $p_t = \omega(r)\rho$, under the condition $p_r = -\rho$. In cases where this latter condition is not satisfied, the model can be generalized to the form $p_i = \omega_i(r)\rho$, thereby indicating how the pressure varies in each spatial direction.

As indicated in Reference [5], a generalized string fluid has a profound impact on galactic scales. In fact, assuming that the transverse pressure of the strings is proportional to their energy density, Reference [6] showed that the force law is modified, thus offering a possible resolution to the flatness problem of spiral galaxy rotation curves [7].

On the other hand, taking as a reference the Kiselev-type equation of state $\bar{p} = \omega(r)\rho$, where \bar{p} denotes the average of the spatial pressures, Reference [5] explores the possibility that a portion of dark matter is not composed of the usual cold dark matter particles of dust-like behavior, but instead takes the form of a generalized string fluid with a cosmic origin and a barotropic factor $\omega = -1/3$. In this context, this particular value of the equation of state is commonly referred to as cosmic strings in various works [8, 9]. The authors of Reference [5] claim that this scenario is consistent with the Hubble diagram of Type Ia supernovae and with data on the gas mass fraction in galaxy clusters. Furthermore, they argue that this mechanism allows for a reduction in the need

for the elusive and thus far undetected cold dark matter.

Wormholes are hypothetical structures that act as shortcuts through spacetime, potentially connecting distant regions of the universe. To remain stable and traversable, such configurations typically require exotic matter – substances that violate the known energy conditions [10, 11]. An intriguing candidate for sustaining wormhole geometries is a cloud of strings – an idealized configuration of one-dimensional defects – which, along with the more general generalized string fluid [12], has been extensively studied in both General Relativity and modified gravity theories [13–17]. A cloud of strings can be understood as a particular case of a generalized string fluid, where the one-dimensional topological defects – fundamental strings or analogs – are aligned in a specific configuration and sparsely distributed throughout spacetime. Unlike a general generalized string fluid, which may possess complex internal dynamics and interactions, a cloud of strings assumes a more idealized, pressureless distribution along some directions, simplifying the energy-momentum tensor and making it a tractable source for analytical solutions.

On the other hand, in the last years have had several proves that indicate that General Relativity (GR) is the correct gravitational theory in four dimensions. Examples of this are the recent detection of gravitational waves through the collision of two rotating black holes [18] or the 2011 Nobel prize about the expansion of the universe. From theoretical point of view this also can be seen through the Lovelock’s theorem [19], which indicates that in four dimensions the General Relativity is the unique theory of gravity because (i) its equations of motion are of second order respect to the metric tensor and (ii) there is diffeomorphism invariance, *i.e.*, the energy momentum is conserved.

However, there are theories of gravity that retain the main features (i) and (ii) of General Relativity. Among them is Lovelock theory [20], in which the Lagrangian includes higher-order corrections—corresponding to terms of order n in the Riemann tensor—to the Einstein-Hilbert action. A particular case of Lovelock theory is Einstein-Gauss-Bonnet (EGB) gravity [21]. The EGB Lagrangian contains three terms in its action, proportional respectively to the cosmological constant ($n = 0$), the Ricci scalar ($n = 1$), and the Gauss-Bonnet term ($n = 2$). It is important to mention that Einstein-Gauss-Bonnet theory has garnered considerable attention in recent years for its applications in inflationary models and has been compared with the observational results from GW170817 [22].

Related to the above, for a long time it was assumed that the Gauss-Bonnet Lagrangian in $d \leq 4$ dimensions does not contribute to the equations of motion, since it corresponds to a total derivative. Thus, in $4D$, this Lagrangian was usually treated as a topological invariant. Conse-

quently, equations of motion in $4D$ for Einstein-Gauss-Bonnet (EGB) gravity only made physical sense in the presence of scalar fields coupled to the aforementioned Lagrangian. Recently, in 2020, in reference [23], it was shown that by re-scaling the coupling constant associated with the Gauss-Bonnet term as $\alpha_2 \rightarrow \alpha/(d-4)$, the Lanczos tensor remains finite and non-zero. As claimed in that reference, this prescription is analyzed from the perspective of classical field theory. In this regard, it is worth mentioning that, as references [24, 25] point out, the existence of solutions in the $4D$ EGB limit does not necessarily imply the existence of a well-defined theory in four dimensions. Several objections have been raised against the $4D$ EGB case [26–28]. However, the conclusion that a four-dimensional Gauss-Bonnet gravity theory does not exist turned out to be premature, as argued in references [24, 25]. It was demonstrated that it is indeed possible to take the limit $D \rightarrow 4$ in the action of EGB [29, 30], generalizing a previous procedure used to take the limit $D \rightarrow 2$ in general relativity [31]. Wormhole solutions in $4D$ EGB gravity have also been explored in the literature. See, for example references [32–37].

Motivated by the ideas previously described, in this work we investigate traversable wormhole solutions in four-dimensional Einstein-Gauss-Bonnet gravity coupled to a generalized string fluid background. We will test the geometric requirements, energy conditions, the volume integral quantifier, and the complexity factor analysis. We will also discuss the nature of the matter sources for the different scenarios considered. In particular, we will examine cases in which the fluid or cloud matter sources resemble quintessence-like, cosmic strings, or exotic matter.

Our paper is structured as follows: In Section II, we review the properties of a generalized string fluid. Section III is dedicated to deriving the wormhole solutions and exploring their geometric characteristics, along with the properties of their source. In Section IV, we analyze the energy conditions and calculate the amount of exotic matter required to sustain the wormhole. Section V focuses on the derivation of the complexity factor. Finally, in Section VI, we present our conclusions.

II. GENERALIZED STRING FLUID

Letelier, in an early work [38], introduced a model to represent a cloud of strings using a surface bivector $\Sigma^{\mu\nu}$. This bivector spans the two-dimensional time-like surface traced by the strings and is defined by

$$\Sigma^{\mu\nu} = \varepsilon^{AB} \frac{\partial x^\mu}{\partial \xi^A} \frac{\partial x^\nu}{\partial \xi^B}, \quad (1)$$

where ε^{AB} is the antisymmetric Levi-Civita symbol in two dimensions, with $\varepsilon^{01} = -\varepsilon^{10} = -1$. The parameters ξ^A , where $A = 0, 1$, represent coordinates on the worldsheet, with ξ^0 being time-like and ξ^1 space-like.

The metric h_{AB} induced on the worldsheet by the spacetime metric $g_{\mu\nu}$ takes the form

$$h_{AB} = g_{\mu\nu} \frac{\partial x^\mu}{\partial \xi^A} \frac{\partial x^\nu}{\partial \xi^B}. \quad (2)$$

Here, the function $x(\xi^A)$ maps the worldsheet trajectory of the strings. Drawing an analogy with the standard energy-momentum tensor for a cloud of particles,

$$T^{\mu\nu} = \rho u^\mu u^\nu, \quad (3)$$

in which ρ denotes the energy density, Letelier suggested substituting $u^\mu u^\nu$ with $\sqrt{-h} \frac{\Sigma^{\mu\lambda} \Sigma_\lambda^\nu}{(-h)}$ [38].

This leads to the expression for the energy-momentum tensor of a string cloud:

$$T^{\mu\nu} = \rho \sqrt{-h} \frac{\Sigma^{\mu\lambda} \Sigma_\lambda^\nu}{(-h)}, \quad (4)$$

where h refers to the determinant of the induced metric h_{AB} . Letelier later generalized this framework to incorporate pressure-like effects [39]. In this extended scenario, the energy-momentum tensor is written as

$$T^{\mu\nu} = (p + \rho \sqrt{-h}) \frac{\Sigma^{\mu\lambda} \Sigma_\lambda^\nu}{(-h)} + p g^{\mu\nu}, \quad (5)$$

with p and ρ representing the pressure and density of the generalized string fluid, respectively. As discussed in [6], the symmetries of the spherically symmetric metric, ensures that $\Sigma_{\mu\lambda}$ has only two nonzero components: Σ_{tr} and $\Sigma_{\theta\varphi}$. Moreover, the determinant h of the induced metric satisfies $h < 0$. These constraints simplify the form of the energy-momentum tensor to

$$T_t^t = T_r^r \quad \text{and} \quad T_\theta^\theta = T_\varphi^\varphi = p. \quad (6)$$

We consider a generalization of the EoS proposed in [6], where $\bar{\alpha}$ to vary with the radial coordinate, i.e.

$$\rho(r) = \bar{\alpha}(r)p(r), \quad (7)$$

leading to the energy-momentum tensor in the form [4]

$$T_\nu^\mu = \left[-\rho(r), -\rho(r), \frac{\rho(r)}{\bar{\alpha}(r)}, \frac{\rho(r)}{\bar{\alpha}(r)} \right]. \quad (8)$$

For the special case corresponding to a pure string cloud, the angular components of pressure vanish. This situation arises in the limit $\bar{\alpha} \rightarrow \infty$, causing $p \rightarrow 0$ in Eq. (8).

In the context of traversable wormhole solutions explored in this work, we consider

$$\bar{\alpha}(r) = \frac{1}{\omega_t(r)}, \quad (9)$$

where $\omega_t(r)$ is the standard linear equation-of-state (EoS) parameter associated with the transverse pressures. Additionally, we relax the black hole condition $\rho(r) = -p_r(r)$ and instead examine the conditions under which

$$\omega_r(r) \rightarrow -1, \quad (10)$$

where $\omega_r(r)$ is the radial linear EoS parameter.

III. WORMHOLE SOLUTIONS: GEOMETRY AND SOURCE PROPERTIES

The Morris-Thorne metric of a Lorentzian traversable wormhole (TWH) is given by [10]

$$ds^2 = -e^{2\Phi(r)}dt^2 + \frac{dr^2}{1 - \frac{b(r)}{r}} + r^2d\Omega^2, \quad (11)$$

where $\Phi(r)$ and $b(r)$ are functions of the radial coordinate r , known as the redshift function and the shape function, respectively. The radial coordinate decreases from infinity to a minimum value r_0 , the radius of the throat, where the boundary condition $b(r_0) = r_0$ must be satisfied. The quantity $d\Omega$ denotes the line element on a unitary 2-sphere.

We have that EGB equations in 4D, for the metric (11), are given by [40–42]

$$8\pi\rho(r) = \frac{b(r)}{r^3} \left(1 - \frac{\alpha b(r)}{r^3}\right) + \frac{1}{r^2} \left(\frac{2\alpha b(r)}{r^3} + 1\right) \left(b'(r) - \frac{b(r)}{r}\right), \quad (12)$$

$$8\pi p_r(r) = -\frac{b(r)}{r^3} \left(1 - \frac{\alpha b(r)}{r^3}\right) + \frac{2}{r} \left(1 - \frac{b(r)}{r}\right) \left(\frac{2\alpha b(r)}{r^3} + 1\right) \Phi'(r), \quad (13)$$

$$\begin{aligned} 8\pi p_t(r) &= -\frac{\alpha b(r)^2}{r^6} + \frac{2\alpha}{r^4} \left(1 - \frac{b(r)}{r}\right) (b(r) - rb'(r)) \Phi'(r) \\ &+ \left(1 - \frac{b(r)}{r}\right) \left(\frac{2\alpha b(r)}{r^3} + 1\right) \left(\frac{(b(r) - rb'(r))\Phi'(r)}{2r(r - b(r))} + \Phi''(r) - \Phi'(r)^2\right) \\ &+ \left(1 - \frac{b(r)}{r}\right) \left(1 - \frac{2\alpha b(r)}{r^3}\right) \left(\frac{b(r) - rb'(r)}{2r^2(r - b(r))} - \frac{\Phi'(r)}{r}\right). \end{aligned} \quad (14)$$

Notice that equation (12) is similar to

$$2 \cdot 4\pi r^2 \rho = b'(r) + \alpha \left(\frac{(b(r)/r)^2}{r} \right)';$$

$$m(r) = \int 4\pi r^2 \rho dr; \quad (15)$$

$$2 \cdot m(r) = b(r) + \frac{\alpha}{r^3} b(r)^2;$$

$$0 = \frac{\alpha}{r^3} b(r)^2 + b(r) - 2m(r);$$

$$b(r) = -\frac{r^3}{2\alpha} \pm \frac{r^3}{2\alpha} \sqrt{1 + \frac{8\alpha}{r^3} m(r)}; \quad (16)$$

$$g_{rr}^{-1} = 1 - \frac{b(r)}{r} = 1 + \frac{r^2}{2\alpha} \left(1 \pm \sqrt{1 + \frac{8\alpha}{r^3} m(r)} \right). \quad (17)$$

In order to recover the general relativity limit we evaluate

$$\lim_{\alpha \rightarrow 0} g_{rr}^{-1} = \lim_{\alpha \rightarrow 0} \left[1 + \frac{r^2}{2\alpha} \left(1 \pm \sqrt{1 + \frac{8\alpha}{r^3} m(r)} \right) \right]$$

$$= \begin{cases} 1 - \frac{2m(r)}{r}, & \text{for the } - \text{ branch} \\ 1 + \frac{2m(r)}{r} + \frac{r^2}{\alpha}, & \text{for the } + \text{ branch} \end{cases} \quad (18)$$

Then we must to take the negative branch in Eq. (17), or equivalently, the positive branch in Eq. (16) in order to recover the general relativity limit. It is worth nothing that the limit with the positive branch in eq 17 is bad defined.

Motivated by reference [4], in this work we study the following energy density model

$$\rho(r) = \frac{\varepsilon a^3 e^{\frac{r^3}{a^3}} + (3\varepsilon r^3 - \varepsilon a^3 + 3r_g r^2)}{8\pi a^3 e^{\frac{r^3}{a^3}} r^2}, \quad (19)$$

where r_g is the Schwarzschild radius, which we set equal to r_0 , namely, the radius of the wormhole throat. Such an energy density acts as the source for a regular black hole, as investigated in [4], and is characterized by the matter distribution of an anisotropic generalized string fluid, with a characteristic scale defined by a . From Eq. (19), it is evident that the energy density increases linearly with ε , and reaches its maximum value at the throat. Consequently, the parameter ε directly quantifies the amount of string fluid present in the spacetime. We can easily see these features in Fig. 1.

Substituting the energy density into Eq. (15), we obtain

$$m(r) = \frac{1}{2} [\beta + \varepsilon r - (\varepsilon r + r_0) \exp(-r^3/a^3)]. \quad (20)$$

Substituting now this mass function into Eq. (16), we get

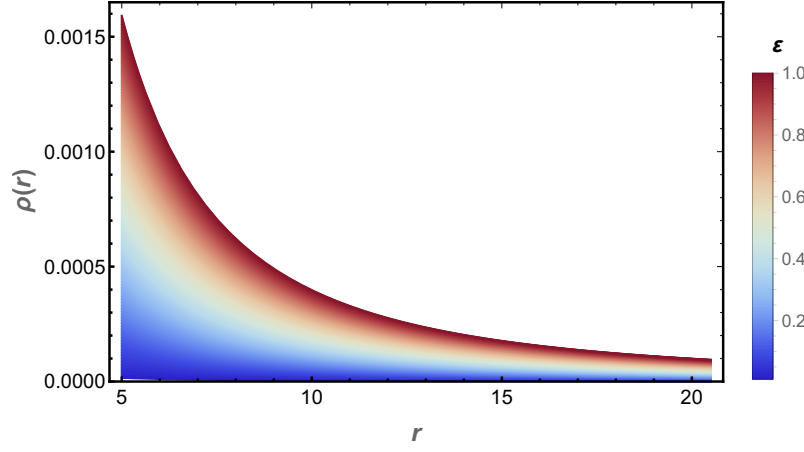


FIG. 1. Color gradient for the energy density $\rho(r)$ for $\varepsilon = [0, 1]$, with $a = 1$ and $r_0 = 5$.

$$b(r) = \frac{r^3}{2\alpha} \left[-1 + \sqrt{1 + \frac{4\alpha}{r^3} \left(\beta + \varepsilon r - (\varepsilon r + r_0) \exp(-r^3/a^3) \right)} \right]. \quad (21)$$

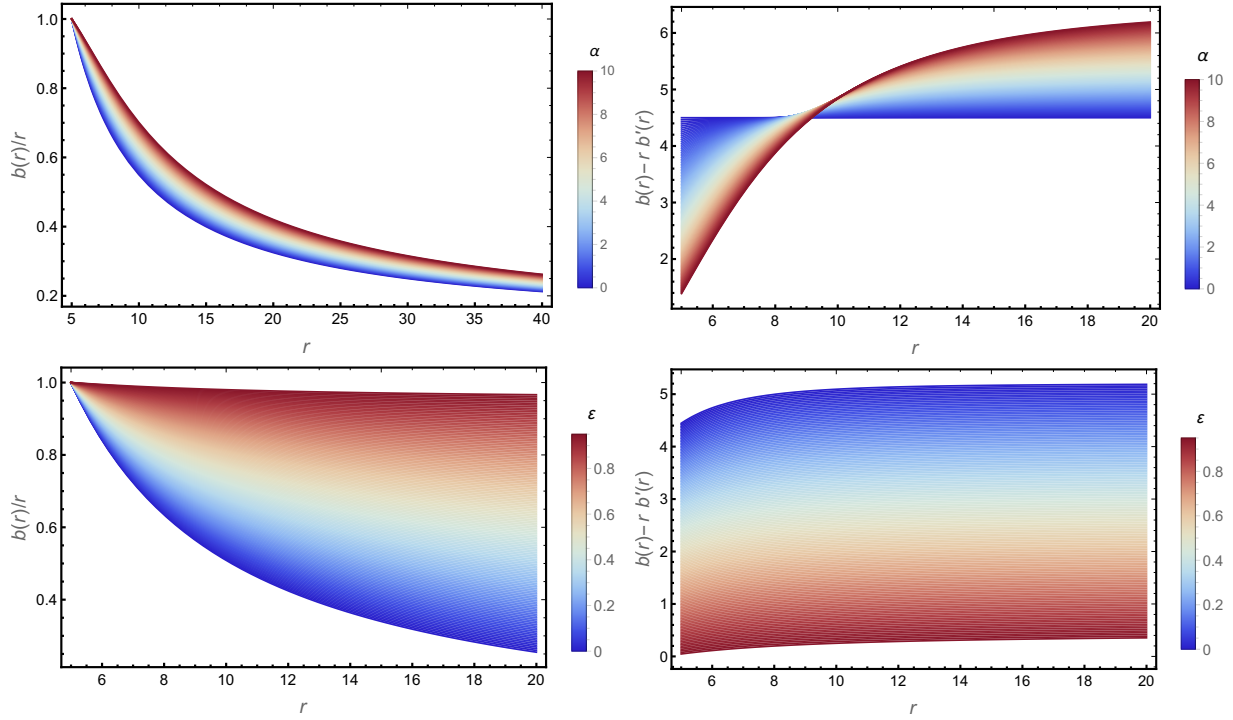


FIG. 2. Top left panel: The geometric condition (2) $b(r)/r$, with $r_0 = 5$, $a = 1$, and $\varepsilon = 0.1$. Top right panel: The geometric condition (4) for $b(r) - rb'(r)$ (flaring-out), considering the same parameters. Bottom left panel: Dependence of $b(r)/r$ on ε , with $r_0 = 5$, $a = 1$, and $\alpha = 0.1$ fixed. Bottom right: Flaring-out condition $b(r) - rb'(r)$ for the same ε -dependent case. In the figures, the color gradient represents $\alpha \in [0, 10]$ (top) and $\varepsilon \in [0, 1]$ (bottom), as shown in the vertical colorbars, respectively.

It is direct to check that

$$\lim_{r \rightarrow \infty} b(r) = \lim_{r \rightarrow \infty} \left[-\frac{r^3}{2\alpha} + \frac{r^3}{2\alpha} \sqrt{1 + \frac{4\alpha}{r^3} [\beta + \varepsilon r - (\varepsilon r + r_0) \exp(-r^3/a^3)]} \right] = 0. \quad (22)$$

Imposing $b(r_0) = r_0$, we find the integration constant as

$$\beta = (1 + \varepsilon)r_0 \exp(-r_0^3/a^3) - r_0(\varepsilon - 1) + \frac{\alpha}{r_0}. \quad (23)$$

Our interpretation of the source for the wormhole solution as a generalized string fluid is well based, as it is easy to verify that, in the limit $\alpha \rightarrow 0$, the term $b(r)/r$ retains a constant value, specifically ε . The presence of this constant in the metric is characteristic of a cloud of strings, a particular case of the generalized string fluid, which is commonly found in black hole solutions, as shown in [4]. Consequently, we recover the GR solution – at least for the radial metric component – sourced by the generalized string fluid when the Gauss–Bonnet coupling α is deactivated.

A. Geometric conditions

The geometric conditions that the shape function and the redshift function must satisfy are:

1. The minimum value of r at the throat of the wormhole corresponds to the point $r = r_0 = b(r_0)$, where the function $g_{rr}^{-1} = 1 - \frac{b(r)}{r}$ vanishes.
2. The proper radial distance

$$l(r) = \pm \int_{r_0}^r \frac{dr}{\sqrt{1 - \frac{b(r)}{r}}}, \quad (24)$$

must be a real number. For this, it is necessary that

$$1 - \frac{b(r)}{r} \geq 0, \quad (25)$$

for all values of $r \geq r_0$.

3. The asymptotic flatness condition requires that

$$\lim_{r \rightarrow \infty} \frac{b(r)}{r} \rightarrow 0. \quad (26)$$

This ensures that at infinity, the proper radial distance $l \rightarrow \pm\infty$.

4. The flaring-out condition, $\frac{b(r) - b'(r)r}{b^2} > 0$, for all values of $r \geq r_0$, ensuring the outward expansion of the TWH throat.

5. The function $\Phi(r)$ must be finite for all values of $r \geq r_0$ in order to avoid singularities and horizons.

The simplest redshift function satisfying condition (5) is a constant, and we shall adopt this choice in the context of the so-called zero-tide wormhole. We now verify whether the geometric conditions

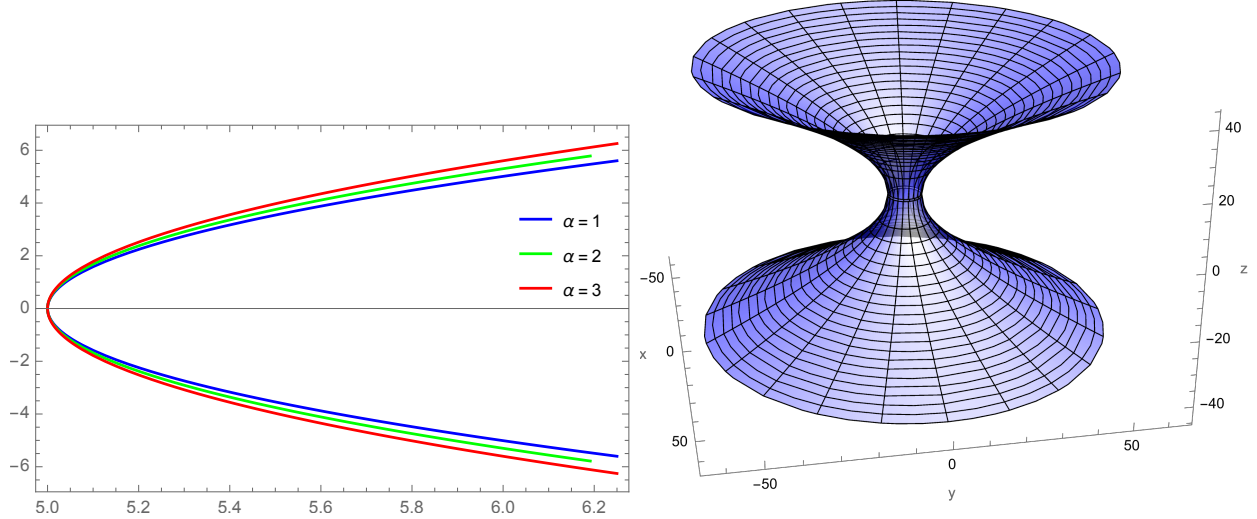


FIG. 3. Left panel: Embedding profiles $z(r)$ of the wormhole in 4D EGB gravity surrounded by a generalized string fluid, plotted for selected values of the coupling constant α . The parameters are set to $r_0 = 5$, $a = 1$, and $\varepsilon = 0.1$. Right panel: Three-dimensional embedding diagram of the wormhole for $\alpha = 0.5$, using the same remaining parameters.

are satisfied by the obtained shape function.

- Conditions (1) and (3) are automatically fulfilled through equations (23) and (22), respectively. So it remains to examine conditions (2) and (4) in detail.
- We analyze condition (2) in figure 2. In the top left panel, we vary α , while in the bottom left panel, we vary ε , keeping the other parameters fixed. Fig. 2, in the top left panel, displays the radial dependence of the metric function ratio $b(r)/r$ across a continuous range of the parameter α , from a null coupling ($\alpha = 0$) to a strong one ($\alpha = 10$). Our analysis reveals that the condition $a < r_0$ emerges as a necessary requirement for satisfying the constraint given by (1). Hence, we can see that the condition (3) is satisfied as well.
- In the top right panel of the same figure, we can easily verify that the geometric condition (4), “flaring-out” is also fulfilled.

The fulfillment of the condition discussed in the previous point is illustrated by the shape of the embedding diagrams shown in Fig. 3, for some values of α . These diagrams are generated from the mapping of the metric spatial sector in cylindrical coordinates at the equatorial plane, via

$$dr^2 + r^2 d\phi^2 + dz^2 = \frac{dr^2}{1 - \frac{b(r)}{r}} + r^2 d\phi^2 \Rightarrow z(r) = \int_{r_0}^r \left[\frac{b(u)/u}{1 - b(u)/u} \right]^{1/2} du. \quad (27)$$

Note that the greater is α , the longer it takes for the wormhole to approach flatness. On the other hand, its curvature appears to be less pronounced at the throat, indicating a smoother transition between the regions connected by the wormhole. This feature is confirmed by the analysis of the curvature scalar made in the next subsection.

B. Curvature

To gain deeper insights into the geometric properties of the wormhole solution, we proceed with the analysis of the curvature, focusing on the Kretschmann scalar $K = R^{\mu\nu\rho\sigma} R_{\mu\nu\rho\sigma}$. This scalar provides a direct measure of the curvature intensity of spacetime, making it a valuable tool for identifying singularities and understanding the influence of the Gauss–Bonnet coupling α and the generalized string fluid parameter ε on the geometry of the wormhole. Thus, in the four-dimensional EGB gravity, the Kretschmann's scalar for the Morris–Thorne wormhole spacetime assumes the following expression

$$K = \frac{4b(r)^2}{r^6} + \frac{2}{r^4} \left(b'(r) - \frac{b(r)}{r} \right)^2 + 8 \left(1 - \frac{b(r)}{r} \right)^2 \frac{\Phi'(r)^2}{r^2} + \left[\left(b'(r) - \frac{b(r)}{r} \right) \frac{\Phi'(r)}{r} - 2 \left(1 - \frac{b(r)}{r} \right) [\Phi''(r) + \Phi'(r)^2] \right]^2. \quad (28)$$

For the zero-tidal wormhole, $\Phi(r) = \text{constant}$, and then we have

$$K = \frac{4b(r)^2}{r^6} + \frac{2}{r^4} \left[b'(r) - \frac{b(r)}{r} \right]^2. \quad (29)$$

According to Fig. 4, the behavior of the Kretschmann curvature reveals fundamental aspects of the wormhole's geometric structure. The scalar remains finite throughout the spacetime, peaking near the throat region and decaying smoothly toward asymptotic infinity, consistent with the solution's regularity and traversability requirements. Both the Gauss–Bonnet coupling α and the generalized fluid density of the string ε modulate its intensity: Larger values of α and lower values of ε reduce the curvature near the throat while enhancing it far from this region due to higher-order gravitational effects. Conversely, higher values of ε and lower values of α similarly decrease

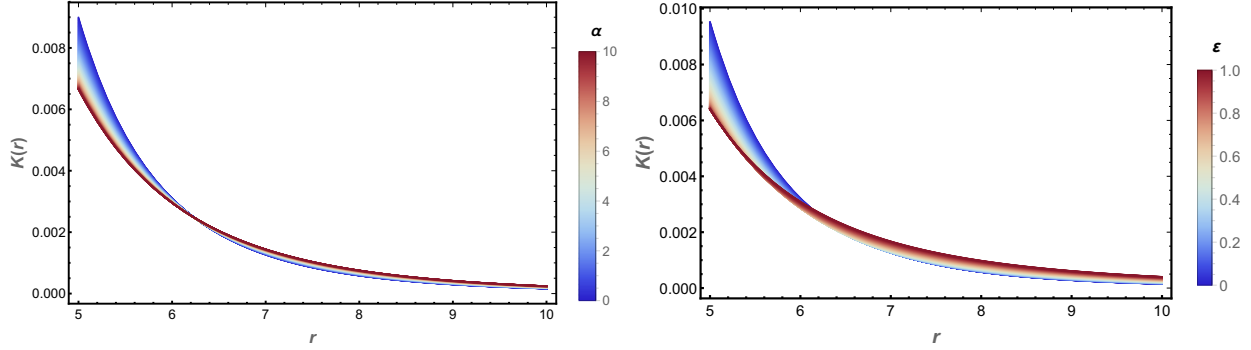


FIG. 4. Left panel: Kretschmann curvature for the wormhole in 4D EGB gravity surrounded by a generalized string fluid, as a function of r . The color gradient shows the Gauss-Bonnet coupling constant in the range $\alpha \in [0, 10]$ (fixed $\varepsilon = 0.1$, $r_0 = 5$, and $a = 1$). Right panel: Kretschmann curvature plotted as a color gradient for $\varepsilon \in [0, 1]$, with fixed $\alpha = 0.1$, $r_0 = 5$, and $a = 1$.

the curvature near the throat but increase it at greater distances. This α - ε interplay maintains finite curvature everywhere, preserving the wormhole's traversability without singularities. The solution's regularity persists across the full parameter space, demonstrating how modified gravity and exotic matter jointly sustain the geometry.

C. Radial and lateral linear equations of state

As expected, our wormhole solution does not satisfy the equation of state (EoS) $\rho(r) = -p_r(r)$, which characterizes a generalized string fluid that supports black hole geometry. To account for this, we examine the behavior of the radial state parameter $\omega_r(r)$, which defines a more general EoS of the form $p_r(r) = \omega_r(r)\rho(r)$, where $\rho(r)$ denotes the density of the generalized string fluid acting as a source for the regular black hole presented in Ref. [4], and given by Eq. (19). The corresponding radial pressure is provided in Eq. (33). In Fig. 5, we plot the radial state parameter $\omega_r(r)$ as a function of r for a continuum of values of α (ε), in the top left panel (top right panel). It is evident that, asymptotically, the relation $p_r = -\rho$ is recovered. Additionally, the parameter $\omega_r(r)$ indicates a phantom-like fluid, since $\omega_r(r) < -1$, with this behavior becoming more pronounced in the vicinity of the wormhole throat. The exoticity becomes less pronounced near the throat for larger values of α , and, for fixed α , it also decreases with increasing ε .

Now we turn to the analysis of the lateral (or tangential) state parameter, defined as $\omega_t(r) = p_t(r)/\rho(r)$, where $p_t = p_\phi = p_\theta$, which represents the second equation of state satisfied by the generalized string fluid [4]. In Fig. 5, we show the behavior of $\omega_t(r)$ as a function of r for a

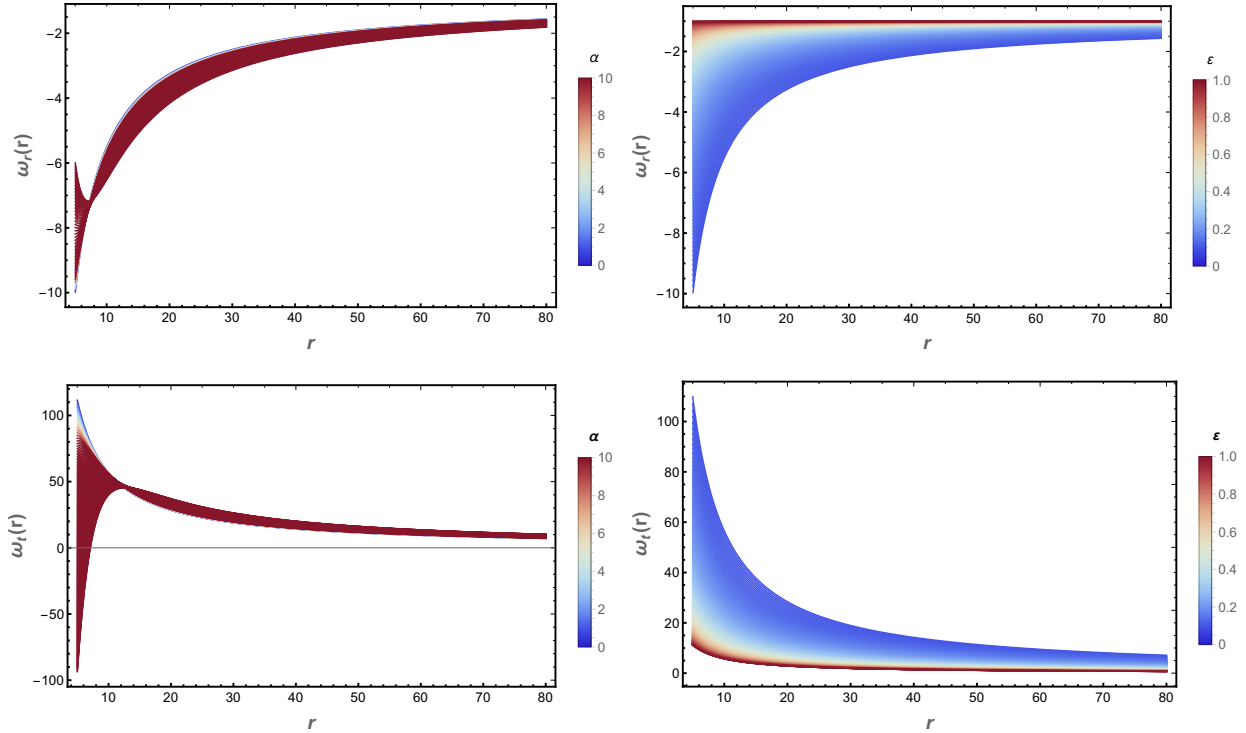


FIG. 5. Radial state parameter $\omega_r(r)$ as a function of r , for $\alpha \in [0, 10]$ (color gradient, top left panel, fixed $\varepsilon = 0.1$). On the top right panel, the color gradient shows the radial state $\omega_r(r)$ for $\varepsilon \in [0, 1]$ (fixed $\alpha = 0.1$). Lateral state parameter $\omega_t(r)$ as a function of the coordinate r , for $\alpha \in [0, 10]$ (bottom left panel, fixed $\varepsilon = 0.1$), and for $\varepsilon \in [0, 1]$ (bottom right panel, fixed $\alpha = 0.1$). In all cases, we have considered $r_0 = 5.0$ and $a = 1.0$.

continuous range of values of α and ε , displayed respectively in the bottom left and bottom right panels. As expected, we observe that $\omega_t(r) \rightarrow 0$ asymptotically, indicating the characteristic behavior of a cloud of strings.

D. Generalized string fluid described by a Kiselev-like source

We now examine the behavior of the linear equation of state (EoS) parameter identified with a Kiselev-like source, which also can be associated with an anisotropic generalized string fluid [4]. We use the fact that

$$\bar{p} = \langle T_j^i \rangle = \frac{p_r + 2p_t}{3} = \omega_q(r)\rho \Rightarrow \frac{p_r + 2p_t}{3\rho} = \omega_q(r). \quad (30)$$

We can check that in the case $p_r = -\rho$, the latter equations reduces to $p_t(r) = \frac{1}{2} [3\omega_q(r) + 1] \rho(r)$. However, this is not our case. On the other hand, the conservation equation is such that

$$(p_r)' + \frac{2}{r}(p_r - p_t) = 0, \\ r(p_r)' + 2p_r = 2p_t. \quad (31)$$

Replacing the above expression in eq. (30)

$$\frac{p_r}{\rho} + \frac{r(p_r)'}{3\rho} = \omega_q(r). \quad (32)$$

From the equation of motion, for the given value of the integration constant β

$$p_r = \frac{1}{8\pi\alpha} + \frac{\alpha + r_0^2(1 - \varepsilon) + r_0r\varepsilon + e^{-\left(\frac{r_0^3}{a^3}\right)}r_0^2(1 + \varepsilon) + e^{-\left(\frac{r_0^3}{a^3}\right)}(-r_0^2 - r_0r\varepsilon)}{8r_0\pi r^3} \\ - \frac{\sqrt{r_0r^3 + 4\alpha^2 + 4e^{-\left(\frac{r_0^3}{a^3}\right)}r_0^2\alpha(1 + \varepsilon) - 4e^{-\left(\frac{r_0^3}{a^3}\right)}r_0\alpha(r_0 + r\varepsilon) + \alpha(r_0^2(4 - 4\varepsilon) + 4r_0r\varepsilon)}}{8\sqrt{r_0}\pi r^{3/2}\alpha}. \quad (33)$$

We can check that

$$\lim_{r \rightarrow \infty} \rho = \lim_{r \rightarrow \infty} p_r = \lim_{r \rightarrow \infty} p_t = 0. \quad (34)$$

This is consistent with the fact that our spacetime is asymptotically flat.

Additionally, as is well known, a quintessence fluid is characterized by the equation of state (EoS) $\bar{p} = \omega_q\rho$, where $\omega_q \in [-1, 0]$ [3]. On one hand, the late time cosmic acceleration of the universe constrains the equation of state of the fluid responsible for this acceleration to lie within the range $\omega_q \in [-1, -1/3]$. On the other hand, the case $\omega_q \in [-1/3, 0]$ is associated with quintessence, such as asymptotically flat spacetimes [43] or black holes exhibiting critical behavior in their thermodynamics [44]. In particular, a value of $\omega_q = -1$ resembles the behavior of a positive cosmological constant, generating, for instance in the Kiselev model [3], a repulsive potential analogous to that produced in a de Sitter spacetime. In this way, $\omega_q = -1$ is associated with a de Sitter-like equation of state.

The condition $\omega_q(r_0) = -1$ (de Sitter-like EoS at the throat) imposes a constraint between the wormhole throat radius r_0 , the string fluid density ε , and the Gauss-Bonnet coupling α . For fixed ε and length scale a , we found that

$$\alpha(r_0) = r_0^2 \left[\frac{\varepsilon(e^{r_0^3/a^3} - 1) + 3(\varepsilon + 1)r_0^3/a^3}{e^{r_0^3/a^3}(3 - 4\varepsilon) + 4\varepsilon - 12(\varepsilon + 1)r_0^3/a^3} \right]. \quad (35)$$

This relation reveals how α must scale with r_0 in order to maintain $\omega_q(r_0) = -1$. Figure 6 (left panel) illustrates this for $\varepsilon = 0.1$ and $a = 1$. The right panel of Fig. 6 confirms that this parameter

choice indeed yields $\omega_q(r_0) = -1$, while asymptotically approaching $\omega_q \rightarrow -1/3$ (cosmic string behavior, dashed line). Notably, this asymptotically approaching limit aligns with observational constraints on late-time cosmic acceleration [3, 8].

Thus, that figures illustrate an example within the parameter space in which the EoS satisfies $\omega_q \in [-1, -1/3]$, *i.e.*, consistent with the constraints associated with the late-time cosmic acceleration of the universe, while the asymptote of the equation of state ($\omega_q \rightarrow -1/3$) resembles the behavior of a cosmic string [8, 9]. Ref. [45] states that a cosmic string can be understood as a long-lived, topologically stable structure that may have been formed during phase transitions in the early Universe. The spacetime around a straight cosmic string is locally flat but globally exhibits a conical topology. The authors assert that the most evident way to detect cosmic strings is through gravitational lensing.

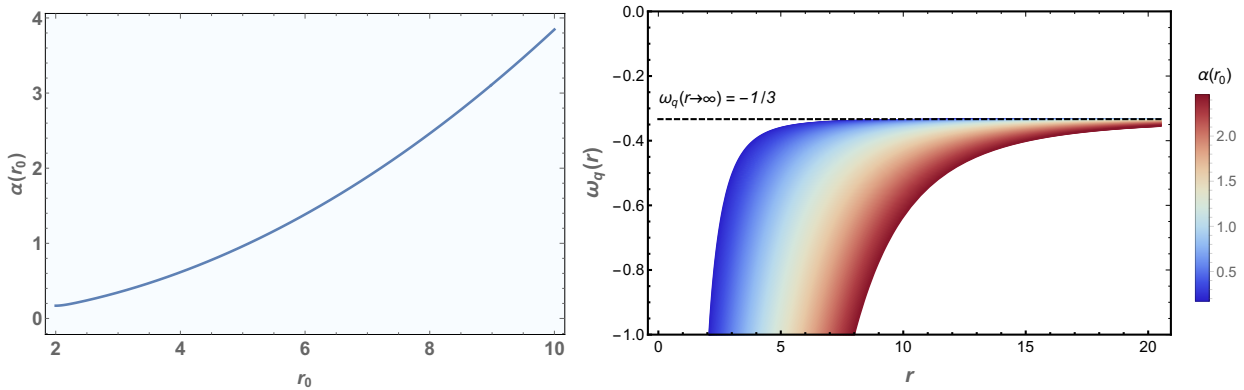


FIG. 6. Left panel: Values of r_0 and $\alpha(r_0)$ in the parameter space such that the equation of state (EoS) near the throat resembles a de Sitter EoS, *i.e.*, $\omega_q(r_0) = -1$. Right panel: Color gradient shows $\omega_q(r)$ for $r_0 \in [2, 8]$. In both cases, we used fixed values of $\varepsilon = 0.1$ and $a = 1$.

IV. NULL ENERGY CONDITION AND QUANTITY OF EXOTIC MATTER

In the study of exotic matter and wormhole solutions, the Null Energy Condition (NEC) plays a fundamental role in ensuring the physical plausibility of such configurations. The NEC can be expressed in terms of the stress-energy tensor components, requiring that the energy density and pressure of any matter distribution satisfy specific inequalities. Specifically, for a static, spherically symmetric spacetime, the NEC is given by the following conditions:

$$\rho + p_r \geq 0, \quad \rho + p_t \geq 0, \quad (36)$$

We will explore here the implications of NEC in the context of the wormhole solutions under consideration. We will analyze how the parameters of the theory, principally the coupling constant α and the generalized string fluid parameter ε , influence the NEC and assess whether any violations of this condition occur in our model, particularly in the strong-coupling regime of Einstein-Gauss-Bonnet gravity.

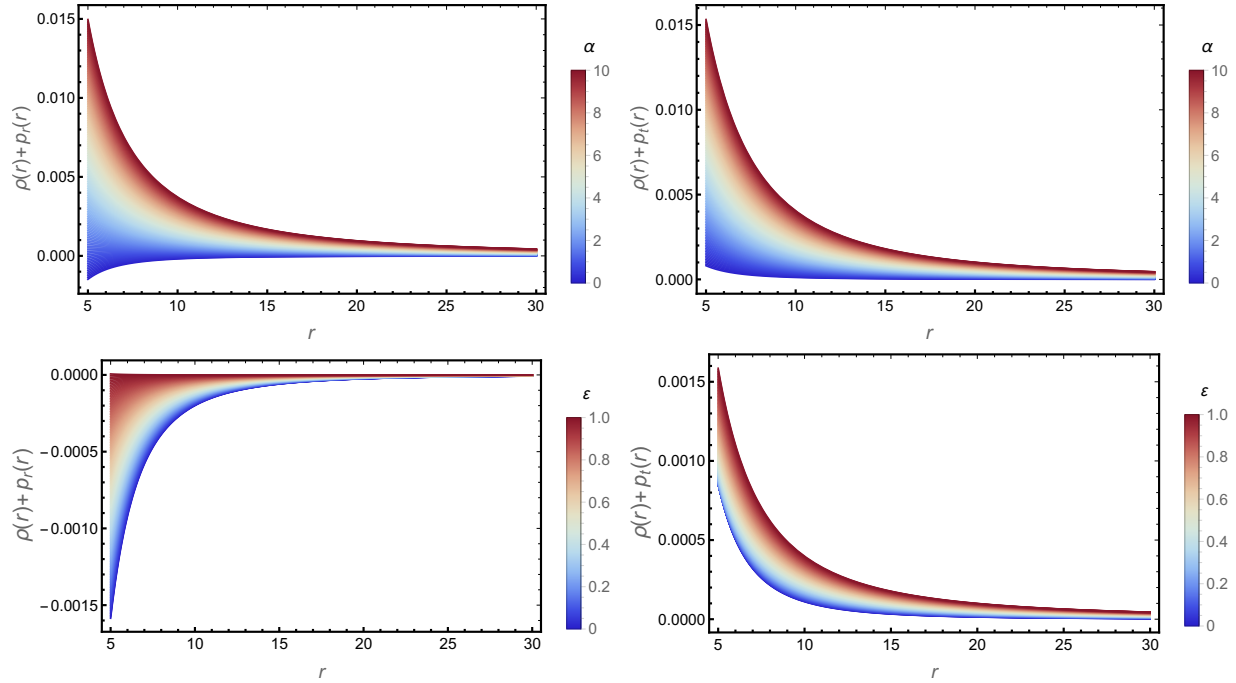


FIG. 7. NEC diagram for the wormhole in EGB surrounded by a generalized string fluid. Top left panel: $\rho(r) + p_r$. Top right panel: $\rho(r) + p_t$, considering several values of α with $r_0 = 5$, $a = 1$, and $\varepsilon = 0.1$. Bottom left panel: $\rho(r) + p_r$ for $\alpha = 0.1$. Bottom right panel: $\rho(r) + p_t$ for $\alpha = 0.1$.

We will analyze now the quantity of exotic matter necessary to sustain the wormhole by calculating the Volume Integral Quantifier (VIQ), defined by [46]

$$\mathcal{I}_v = \oint 4\pi r^2(\rho + p_r) dr = 2 \int_{r_0}^r 4\pi x^2(\rho + p_r) dx. \quad (37)$$

Here, we are particularly interested in evaluating this quantity near the wormhole throat. Although wormhole geometries are generally associated with violations of the null energy condition (NEC), our analysis reveals that for sufficiently high values of the Einstein-Gauss-Bonnet (EGB) coupling and low values of the generalized string fluid parameter, the NEC may remain satisfied in the vicinity of the throat. In such cases, the integral \mathcal{I}_v can approach zero or even become positive, suggesting that the wormhole could be supported without the need for exotic matter in this regime.

This highlights the role of higher-curvature corrections and exotic fluids in modifying classical energy condition requirements.

Using Eqs. (12) and (13), and expanding the integrand of Eq. (37) to first order around $r = r_0$, we find that the Volume Integral Quantifier (VIQ) is approximately given by

$$\mathcal{I}_v \approx \left[-1 + \frac{3e^{-r_0^3/a^3}r_0}{8a^3\pi} + \frac{\alpha}{r_0^2} + \left(\frac{1}{8\pi r_0^2} - \frac{e^{-r_0^3/a^3}}{8\pi r_0^2} + \frac{3e^{-r_0^3/a^3}r_0}{8a^3\pi} \right) \varepsilon \right] (r - r_0). \quad (38)$$

This expression shows that, for fixed values of ε , r_0 , and a , the VIQ evaluated near the wormhole throat can be made arbitrarily small by increasing the coupling constant α . This suggests that the total amount of exotic matter required to sustain the wormhole may become negligible in the strong-coupling regime of Einstein-Gauss-Bonnet gravity, as already demonstrated in the previous analysis concerning the radial state parameter.

V. COMPLEXITY FACTOR

The complexity factor is a scalar quantity that encapsulates the degree of structural inhomogeneity and pressure anisotropy within a self-gravitating system. Originally introduced by Herrera [47], it provides a geometric and physical measure of the internal intricacies of a spacetime configuration. In the context of wormholes, especially those supported by exotic matter or non-standard sources, the complexity factor offers insights into the interplay between matter distribution and curvature. In this section, we analyze the complexity factor associated with a wormhole solution in EGB gravity, sustained by a generalized string fluid source, to assess how higher-curvature corrections, anisotropic stresses, and inhomogeneous density influence the internal structure of the configuration. The complexity factor is thus defined by

$$Y_{TF} = 8\pi(p_r - p_t) - \frac{4\pi}{r^3} \int_{r_0}^r u^3 \frac{d\rho(u)}{du} du. \quad (39)$$

Interestingly, a zero complexity factor implies a non-local equation of state, a condition that does not apply to our wormhole configuration. In fact, through Fig. 8, left panel, we can see that as the Gauss-Bonnet coupling α increases, the complexity factor decreases in magnitude throughout the radial domain, but without reaching the null value. This trend is especially pronounced near the wormhole throat. Such a behavior suggests that the higher-curvature corrections introduced by the Gauss-Bonnet term act to simplify the underlying gravitational configuration. Physically, this may indicate that wormhole geometries in EGB gravity require less structural support from exotic matter as the contribution from the Gauss-Bonnet term becomes dominant. This supports

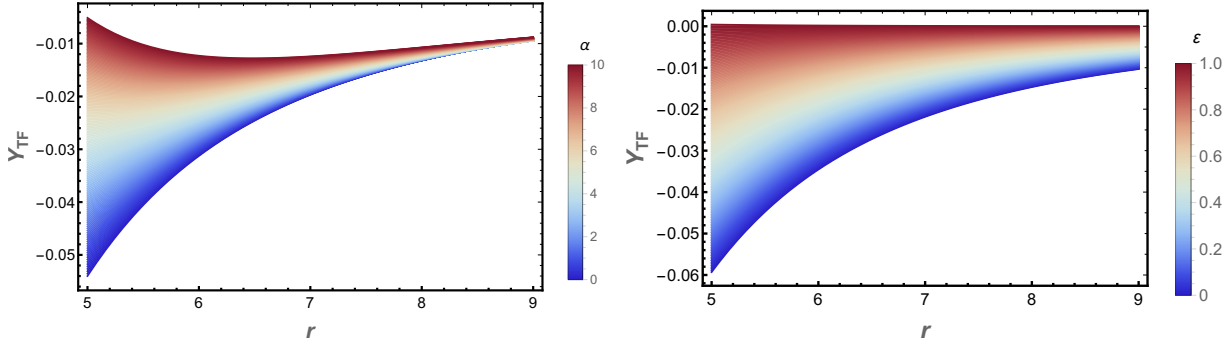


FIG. 8. Left panel: Radial profile of the complexity factor for fixed generalized string fluid parameter ($\varepsilon = 0.1$) and varying Gauss-Bonnet coupling α . Right panel: Dependence on the generalized string fluid parameter ε at fixed $\alpha = 0.1$, showing the same quantity. All functions are computed for characteristic parameters $r_0 = 5.0$ and length scale $a = 1.0$.

the interpretation that the presence of nonlinear curvature terms in the EGB action introduces a smoothing effect on the wormhole geometry, reducing the impact of factors that would otherwise increase its complexity.

On the other hand, an increase in the string fluid content, modeled by a higher value of the parameter ε , also leads to a decrease in the magnitude of the complexity factor for a fixed Gauss–Bonnet coupling α , as illustrated in the right panel of the same figure 8. This feature suggests that the presence of anisotropic stresses associated with the generalized string fluid contributes to reducing the gravitational complexity of the wormhole structure, with a more pronounced distribution of strings tending toward more isotropic behavior. The limit situation $\varepsilon \rightarrow 1$ leads to $Y_{TF} \rightarrow 0$ in all spacetime.

Thus, the combined effect of the generalized string fluid and higher-curvature corrections appears to facilitate the maintenance of the wormhole geometry with reduced energetic or structural demands.

VI. CONCLUSION

Our investigation of traversable wormholes in four-dimensional Einstein-Gauss-Bonnet gravity with a generalized string fluid background has yielded several important theoretical insights. The novel solution we obtained satisfies all fundamental requirements for a traversable wormhole, with the shape function $b(r)$ properly defining the geometric structure, and the simplest chosen redshift function $\Phi(r)$ characterizing a zero tidal wormhole ensures the absence of horizons and singularities.

The embedding diagrams reveal how the wormhole geometry depends on the Gauss-Bonnet coupling α , with larger values producing a more gradual approach to flatness while reducing curvature at the throat region, all while maintaining a smooth, singularity-free geometry.

The most significant finding concerns the behavior of the null energy condition (NEC). While wormholes in classical general relativity typically require exotic matter that violates the NEC, our analysis reveals that in this EGB framework with generalized string fluid background, the NEC can be satisfied in substantial regions of spacetime. Specifically, for parameter ranges with small generalized string fluid density ($\varepsilon \lesssim 0.1$) and strong Gauss-Bonnet coupling ($\alpha \gtrsim 1$), both radial and transverse NEC components $\rho + p_r$ and $\rho + p_t$ remain non-negative outside the immediate throat region. This represents a remarkable feature of higher-curvature gravity theories, demonstrating their potential to support wormhole geometries while reducing reliance on exotic matter.

The regular behavior of the Kretschmann curvature confirms the geometric consistency of our wormhole solution, with finite values maintained throughout the spacetime. The curvature profile demonstrates a clear interplay between the higher-order gravitational effects (governed by α) and matter content (controlled by ε). Larger values of α and lower values of ε , or vice versa, reduce the curvature near the throat while enhancing it far from the throat. This balanced dependence between the parameters ensures the solution remains singularity-free while allowing modulation of the local curvature structure, further supporting the physical viability of these wormhole geometries in Einstein-Gauss-Bonnet gravity coupled to generalized string fluids.

Analysis of the linear state parameter, namely the radial and lateral ones, revealed that the parameter configuration that brings the wormhole matter source closer to a pure string cloud corresponds to the regime where the Gauss-Bonnet coupling is small and the generalized string fluid parameter ε approaches its maximum value allowed by the wormhole geometry, that is, $\varepsilon \sim 1$.

Our analysis has shown that the Volume Integral Quantifier (VIQ), which represents the total amount of exotic matter needed to support the wormhole, can be significantly reduced in the vicinity of the throat by increasing the coupling constant α , as the geometric conditions required for the wormhole's stability remain valid. This behavior is in agreement with the non-violation of NEC in the region near the throat, as previously discussed, further strengthening the physical plausibility of such wormhole configurations.

Our analysis also demonstrated that both the Gauss-Bonnet coupling α and generalized string fluid parameter, ε , significantly reduce the magnitude of the wormhole complexity factor, particularly near the throat. As shown in Fig. 8, stronger Gauss-Bonnet effects diminish the gravitational complexity, suggesting a reduced requirement for exotic matter to sustain the wormhole geome-

try. A larger quantity of generalized string fluid, parametrized by ε , exhibits a similar simplifying effect at fixed and low values for α . The synergistic action of these mechanisms indicates that higher-curvature corrections and exotic matter components can cooperatively maintain traversable wormholes with lower energetic costs. These results provide important insights into how modified gravity theories and non-standard matter content may facilitate stable wormhole configurations.

These results have important implications for theoretical studies of exotic spacetime structures in modified gravity. They demonstrate concretely how higher-curvature terms can alter the energy conditions required to sustain wormholes, potentially making such solutions more physically plausible. The generalized string fluid background plays a crucial stabilizing role in this scenario. Future research directions should include stability analysis under perturbations, investigation of possible observational signatures in gravitational wave astronomy, extension to rotating solutions, and exploration of the thermodynamic aspects in relation to black hole physics. The present work opens several promising avenues for understanding how string-inspired gravity modifications might allow for traversable wormhole solutions with reduced exotic matter requirements.

Acknowledgments. This work was supported by Conselho Nacional de Desenvolvimento Científico e Tecnológico (CNPq) and Fundação Cearense de Apoio ao Desenvolvimento Científico e Tecnológico (FUNCAP). LCNS would like to thank FAPESC for financial support under Grant No. 735/2024. The authors thank colleagues at Universidade Estadual do Ceará for valuable discussions.

- [1] R. R. Caldwell, R. Dave, and P. J. Steinhardt, *Phys. Rev. Lett.* **80**, 1582 (1998), arXiv:astro-ph/9708069.
- [2] P. J. E. Peebles and B. Ratra, *Rev. Mod. Phys.* **75**, 559 (2003), arXiv:astro-ph/0207347.
- [3] V. V. Kiselev, *Class. Quant. Grav.* **20**, 1187 (2003), arXiv:gr-qc/0210040.
- [4] L. C. N. Santos, *Phys. Rev. D* **111**, 064032 (2025), arXiv:2502.15846 [gr-qc].
- [5] S. Capozziello, V. F. Cardone, G. Lambiase, and A. Troisi, *Int. J. Mod. Phys. D* **15**, 69 (2006), arXiv:astro-ph/0601266.
- [6] H. H. Soleng, *Gen. Rel. Grav.* **27**, 367 (1995), arXiv:gr-qc/9412053.
- [7] Y. Sofue and V. Rubin, *Ann. Rev. Astron. Astrophys.* **39**, 137 (2001), arXiv:astro-ph/0010594.
- [8] A. Vilenkin, *Phys. Rev. D* **24**, 2082 (1981).
- [9] R. J. Nemiroff and B. Patla, *Am. J. Phys.* **76**, 265 (2008), arXiv:astro-ph/0703739.

[10] M. S. Morris and K. S. Thorne, Am. J. Phys. **56**, 395 (1988).

[11] M. Visser, *Lorentzian Wormholes: From Einstein to Hawking* (AIP Press, 1995).

[12] S. Arshad and U. Sheikh, Int. J. Theor. Phys. **63**, 90 (2024).

[13] M. G. Richarte and C. Simeone, Int. J. Mod. Phys. D **17**, 1179 (2008), arXiv:0711.2297 [gr-qc].

[14] U. Sheikh, S. Arshad, and R. Pincak, Can. J. Phys. **101**, 525 (2023).

[15] G. Mustafa, F. Javed, S. K. Maurya, and S. Ray, Chin. J. Phys. **88**, 32 (2024), arXiv:2211.10778 [gr-qc].

[16] D. J. Gogoi and U. D. Goswami, JCAP **02**, 027 (2023), arXiv:2208.07055 [gr-qc].

[17] A. Waseem, F. Javed, M. Z. Gul, G. Mustafa, and A. Errehymy, Eur. Phys. J. C **83**, 1088 (2023).

[18] B. P. Abbott *et al.* (LIGO Scientific, Virgo), Phys. Rev. Lett. **116**, 061102 (2016), arXiv:1602.03837 [gr-qc].

[19] D. Lovelock, J. Math. Phys. **13**, 874 (1972).

[20] D. Lovelock, J. Math. Phys. **12**, 498 (1971).

[21] D. G. Boulware and S. Deser, Phys. Rev. Lett. **55**, 2656 (1985).

[22] V. K. Oikonomou, Class. Quant. Grav. **38**, 195025 (2021), arXiv:2108.10460 [gr-qc].

[23] D. Glavan and C. Lin, Phys. Rev. Lett. **124**, 081301 (2020), arXiv:1905.03601 [gr-qc].

[24] M. Gammon and R. B. Mann, Phys. Rev. D **110**, 044004 (2024), arXiv:2210.01909 [gr-qc].

[25] M. Gammon, S. Rourke, and R. B. Mann, Phys. Rev. D **109**, 024026 (2024), arXiv:2309.00703 [gr-qc].

[26] M. Gürses, T. c. Şışman, and B. Tekin, Eur. Phys. J. C **80**, 647 (2020), arXiv:2004.03390 [gr-qc].

[27] W.-Y. Ai, Commun. Theor. Phys. **72**, 095402 (2020), arXiv:2004.02858 [gr-qc].

[28] F.-W. Shu, Phys. Lett. B **811**, 135907 (2020), arXiv:2004.09339 [gr-qc].

[29] R. A. Hennigar, D. Kubiznák, R. B. Mann, and C. Pollack, JHEP **07**, 027 (2020), arXiv:2004.09472 [gr-qc].

[30] P. G. S. Fernandes, P. Carrilho, T. Clifton, and D. J. Mulryne, Phys. Rev. D **102**, 024025 (2020), arXiv:2004.08362 [gr-qc].

[31] R. B. Mann and S. F. Ross, Class. Quant. Grav. **10**, 1405 (1993), arXiv:gr-qc/9208004.

[32] K. Jusufi, A. Banerjee, and S. G. Ghosh, Eur. Phys. J. C **80**, 698 (2020), arXiv:2004.10750 [gr-qc].

[33] A. Dixit, C. Chawla, and A. Pradhan, Int. J. Geom. Meth. Mod. Phys. **18**, 2150064 (2021), arXiv:2005.03985 [physics.gen-ph].

[34] C.-Y. Zhang, C. Niu, W.-L. Qian, X. Wang, and P. Liu, Chin. J. Phys. **83**, 527 (2023), arXiv:2004.14267 [gr-qc].

[35] P. Liu, C. Niu, and C.-Y. Zhang, Chin. Phys. C **45**, 025111 (2021).

[36] A. K. Mishra, Shweta, and U. K. Sharma, Pramana **96**, 218 (2022), arXiv:2106.04369 [gr-qc].

[37] N. Godani, Int. J. Geom. Meth. Mod. Phys. **21**, 2450227 (2024).

[38] P. S. Letelier, Physical Review D **20**, 1294 (1979).

[39] P. S. Letelier, Il Nuovo Cimento B (1971-1996) **63**, 519 (1981).

[40] M. Farooq and M. Zubair, Annals Phys. **459**, 169542 (2023).

- [41] M. Chakraborty and S. Chakraborty, Phys. Dark Univ. **47**, 101793 (2025).
- [42] M. S. Cunha, M. O. Tahim, and C. R. Muniz, Commun. Theor. Phys. **77**, 085402 (2025).
- [43] S. G. Ghosh, S. U. Islam, and S. D. Maharaj, Phys. Scripta **99**, 065032 (2024), arXiv:2307.11611 [gr-qc].
- [44] V. B. Bezerra, I. P. Lobo, J. P. Moraes Graça, and L. C. N. Santos, Eur. Phys. J. C **79**, 949 (2019).
- [45] I. Fernández-Núñez and O. Bulashenko, Phys. Lett. A **380**, 2897 (2016), arXiv:1605.03176 [astro-ph.CO].
- [46] K. K. Nandi, Y.-Z. Zhang, and K. B. Vijaya Kumar, Phys. Rev. D **70**, 127503 (2004), arXiv:gr-qc/0407079.
- [47] L. Herrera, Phys. Rev. D **97**, 044010 (2018), arXiv:1801.08358 [gr-qc].